Encoding daily rainfall records via adaptations of the fractal multifractal method

M. L. Maskey, C. E. Puente, B. Sivakumar & A. Cortis

Stochastic Environmental Research and Risk Assessment

ISSN 1436-3240

Stoch Environ Res Risk Assess
DOI 10.1007/s00477-015-1201-7

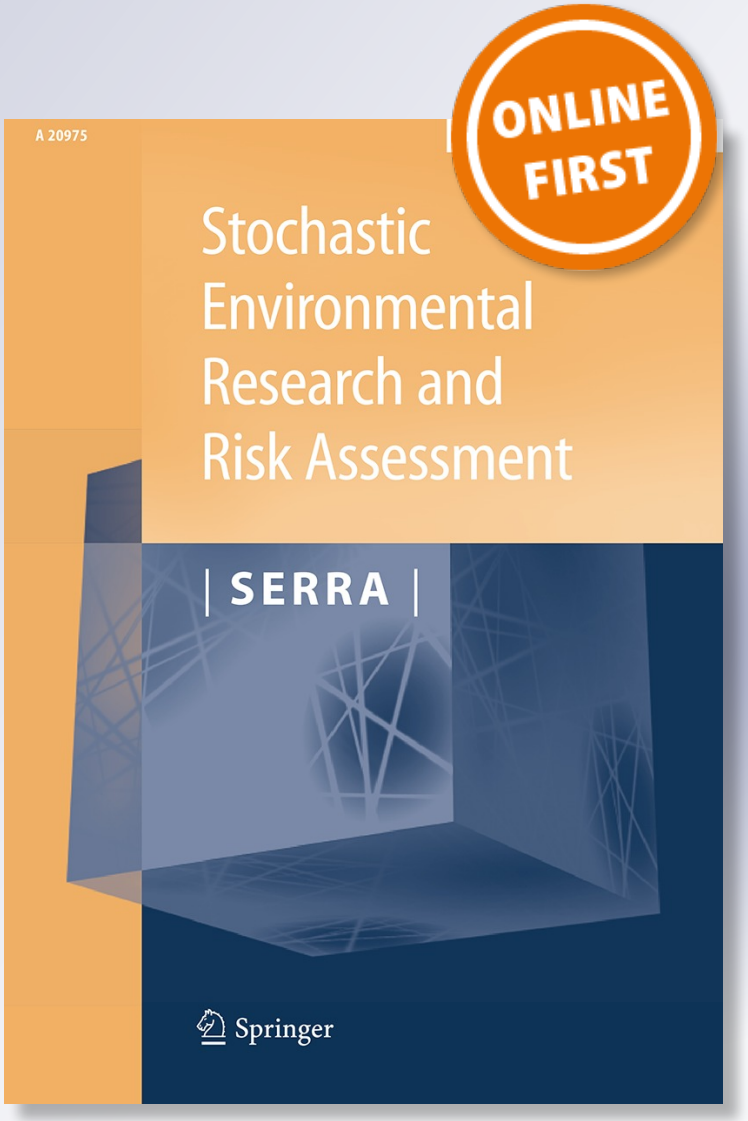

Springer

Stoch Environ Res Risk Assess
DOI 10.1007/s00477-015-1201-7

ORIGINAL PAPER

Encoding daily rainfall records via adaptations of the fractal multifractal method

M. L. Maskey[1] · C. E. Puente[1] · B. Sivakumar[1,2] · A. Cortis[3]

Abstract A deterministic geometric approach, the fractal–multifractal (FM) method, already found useful in modeling storm events, is adapted here in order to encode, for the first time, highly intermittent daily rainfall records gathered over a water year and containing many days of zero rain. Through application to data sets gathered at Laikakota in Bolivia and Tinkham in Washington, USA, it is demonstrated that the modified FM approach can represent erratic rainfall records faithfully, while using only a few FM parameters. It is shown that the modified FM approach, by capturing the rain accumulated over the season, ends up preserving other statistical attributes as well as the overall "texture" of the records, leading to FM sets that are indistinguishable from observed sets and certainly within the limits of accuracy of measured rainfall. This fact is further corroborated comparing 20 consecutive years at Laikakota and a modified FM representation, via common statistical qualifiers, such as histogram, entropy function, and inter-arrival times.

Keywords Rainfall · Encoding · Simulation · Intermittency · Fractals · Complexity · Fractal–multifractal approach · Inverse problem · Particle swarm optimization

Abbreviations

RMSEAR	Root mean square error in accumulated rainfall (observed vs. FM fitted)
MAXEAR	Maximum error in accumulated rainfall (observed vs. fitted)
NSR7	Nash–Sutcliffe statistic between observed rainfall at the weekly scale (observed vs. fitted)
NSACR	Nash–Sutcliffe statistic between rainfall autocorrelations (observed vs. fitted)
AL0	Lag where autocorrelation reaches zero for the first time
NSHR	Nash–Sutcliffe statistic between rainfall histograms (observed vs. fitted)
PZMR	Percent of zeros matched between observed and fitted rainfalls
PF90	Percent histogram mass in fitted records corresponding to 90 % in observed data
NSER	Nash–Sutcliffe statistic between rainfall entropies (observed vs. fitted)

1 Introduction

Since the advent of modern computational power, a number of scientists have been making a substantial effort in conceptualizing numerous physical and stochastic hydrologic models in order to represent both the temporal and the spatial variability of the hydrologic phenomena. Typically, as it happens with rainfall measurements, information is complex in nature and its random-looking appearance has resulted in approaches that aim at finding meaningful geophysical parameters to describe such data sets. Even

✉ C. E. Puente
cepuente@ucdavis.edu

[1] Department of Land, Air & Water Resources, University of California, Davis, CA 95616, USA

[2] School of Civil and Environmental Engineering, The University of New South Wales, Sydney, NSW 2052, Australia

[3] GE Oil & Gas, Houston, TX 77032, USA

Published online: 23 December 2015

though these (stochastic) models preserve some statistics of the records, these approximate parameterizations, based on simplified assumptions, are typically not capable of capturing some finer details, such as the specific intermittency present in the sets.

During the past two decades, researchers have become concerned with the possible chaotic nature of rainfall and other geophysical records (e.g. Rodriguez-Iturbe et al. 1989; Jayawardena and Lai 1994; Puente and Obregón 1996; Sivakumar et al. 2001, 2014; Jin et al. 2005; Kim et al. 2009; Sivakumar and Singh 2012; Jothiprakash and Fathima 2013); see Sivakumar (2000, 2004, 2009) for reviews. Following the lead of the late great mathematician Benoit Mandelbrot, who introduced fractal geometry, several methods have been devised to analyze geophysical records that exhibit the trait of self-similarity. In his seminal works, Mandelbrot (1982, 1989) explained how such self-similarity may bridge the gaps among various temporal and spatial scales and how the concept of multifractals may further help to understand the organization of natural patterns; see also Feder (1988). Several researchers (e.g. Rodriguez-Iturbe 1986; Gupta and Waymire 1990; Tessier et al. 1993) have implemented stochastic (fractal) theories in trying to understand the erratic, intermittent, complex, or, as mentioned earlier, "seemingly random" nature of rainfall records. Even though success has been attained in producing suitable realizations of rainfall via the so-called "universal multifractals" (e.g. Lovejoy and Schertzer 2013), the precise locations of textures present in data are indeed difficult to capture. In recent years, there have also been a number of attempts to use wavelets for studying scaling and related properties of rainfall and other hydrologic processes (e.g. Kumar and Foufoula-Georgiou 1993; Labat et al. 2000; Labat 2008; Niu and Chen 2010; Mishra et al. 2011).

Aiming at developing a geometric approach to natural complexity, Puente (1996) introduced the fractal–multifractal (FM) method, establishing that such an approach was capable of generating random looking sets, as in nature, but modeled as fractal transformation of multifractal measures. Such an approach produces indeed a vast class of patterns defined over one and higher dimensions that preserve some key statistical indicators, viz. moments, autocorrelation function, power spectrum, multifractal spectrum, including, in a welcoming manner, some of the textures present in the data sets, which, as mentioned before, are quite difficult to preserve via physical and stochastic models.

Inspired by the advent of chaos theory (e.g., Lorenz 1963) and by its usage to model precipitation (e.g., Rodriguez-Iturbe et al. 1989), Puente and Obregón (1996), Puente et al. (2001a, b), and Puente and Sivakumar (2007) showed that the FM method was able to capture hidden order in the dynamics of geophysical sets and demonstrated fruitful applications of such methodology for different rainfall sets gathered every few seconds (e.g., Puente and Obregón 1996; Cortis et al. 2009, 2010, 2013; Huang et al. 2012). Indeed, the deterministic FM methodology may generate complex-looking sets with a relatively small number of parameters, and this happens despite the fact that the associated parameter-space is rather intricate, hence requiring a suitable optimization approach for a given set (Huang et al. 2012, 2013).

This paper enlightens, for the first time, the application of the FM method for encoding highly intermittent precipitation records containing many instances of zero rain, i.e., sets beyond individual events lasting few hours as done before. Specifically, this study introduces adaptations of the original FM approach and then uses them to encode four precipitation data sets measured daily and for the extent of a water year: two sets gathered in Laikakota, Bolivia for 273 days and two others measured at Tinkham, Washington, USA for 365 days. With the ideas fully explained and the 4 years fully analyzed, the notions are then extended for a 20 year period in Laikakota. Having introduced a physical interpretation of the FM approach as a realization of a non-trivial multiplicative cascade (Cortis et al. 2013), this work represents a relevant application with highly complex data sets that are rather difficult to harness.

The organization of this paper is as follows. Section 2 reviews the original FM approach and a generalized version of it and presents the adaptations used to encode the complex intermittent sets considered in this study. Section 3 explains the inverse problem strategy employed on a given data set. Section 4 shows the results obtained for two data sets each gathered in Bolivia and Washington, USA, including a variety of statistical attributes. Section 5 compares 20 contiguous years at Laikakota and an adapted FM representation obtained encoding the records year by year. Section 6 includes the concluding remarks.

2 The fractal multifractal approach

2.1 The original method

In its earliest form, Puente (1996) proposed modeling observed records by computing the projection (derived distribution) made by the graphs of fractal interpolating functions when "illuminated" by suitable multifractal measures. These two components are explained next.

Following Barnsley (1988), a *fractal interpolating function* f: $x \rightarrow y$ passing through $N + 1$ ordered points on the plane $\{(x_n, y_n)|x_0 < x_1 \cdots < x_N\}$, and hence having as

its graph the set $G = \{(x, f(x)\,|x \in [0,1]\}$, is defined as the unique fixed point of N simple affine maps of the form:

$$w_n\begin{pmatrix} x \\ y \end{pmatrix} = \begin{pmatrix} a_n & 0 \\ c_n & d_n \end{pmatrix}\begin{pmatrix} x \\ y \end{pmatrix} + \begin{pmatrix} e_n \\ f_n \end{pmatrix} \quad n = 1, \ldots, N, \tag{1}$$

that is, $G = w_1(G) \cup w_2(G) \cup \cdots w_N(G)$.

In these equations, d_n, the so-called vertical scaling parameters, satisfy $|d_n| < 1$ while the other parameters, a_n, c_n, e_n and f_n, are evaluated by imposing contracting initial conditions that guarantee the existence of function f, namely:

$$w_n\begin{pmatrix} x_0 \\ y_0 \end{pmatrix} = \begin{pmatrix} x_{n-1} \\ y_{n-1} \end{pmatrix}, \quad w_n\begin{pmatrix} x_N \\ y_N \end{pmatrix} = \begin{pmatrix} x_n \\ y_n \end{pmatrix}. \tag{2}$$

These last set of equations gives rise to simple linear systems of equations for the "other" parameters in terms of the vertical scaling parameters and the coordinates of the interpolating points. At the end, such maps define a convoluted "wire" function f whose graph has a fractal dimension $1 \leq D < 2$.

A fractal function may be produced via a point-wise sampling of the "attractor" G iterating successively the affine maps. This process, known as the "chaos game" (Barnsley 1988), starts at a point within G (say, an interpolating point) and progresses guided by arbitrary "coin tosses" that assign distinct usage proportions to the N maps. Allowing enough time for the iterations, the process not only paints a graph G point by point but also induces a unique invariant measure over G, which typically contains intermittencies and possesses multifractal properties.

Seen over the coordinate x, such invariant measures define *deterministic multinomial multifractals*—with length scales given by the placements of the interpolating points in x and with the proportions for the "coin tosses" defining the intermittencies—(e.g. Mandelbrot 1989; Puente 1996). When seen over the coordinate y, the invariant measures over G define deterministic projections, which turn out to encompass some of the irregular shapes encountered in nature, such as, we shall see, intermittent rainfall sets gathered over days.

Figure 1 shows an example of these notions for a fractal wire f passing through the four interpolating points $\{(0,0), (0.35, -1.26), (0.79, 3.51), (1,1)\}$, as shown by bullets, and obtained via 2^{14} iterations of the following three affine maps:

$$w_1\begin{pmatrix} x \\ y \end{pmatrix} = \begin{pmatrix} 0.35 & 0 \\ -1.44 & 0.18 \end{pmatrix}\begin{pmatrix} x \\ y \end{pmatrix} \tag{3}$$

$$w_2\begin{pmatrix} x \\ y \end{pmatrix} = \begin{pmatrix} 0.44 & 0 \\ 4.47 & 0.30 \end{pmatrix}\begin{pmatrix} x \\ y \end{pmatrix} + \begin{pmatrix} 0.35 \\ -1.26 \end{pmatrix} \tag{4}$$

$$w_3\begin{pmatrix} x \\ y \end{pmatrix} = \begin{pmatrix} 0.21 & 0 \\ -2.09 & -0.42 \end{pmatrix}\begin{pmatrix} x \\ y \end{pmatrix} + \begin{pmatrix} 0.79 \\ 3.51 \end{pmatrix} \tag{5}$$

according to the proportions, in order, 48, 11, and 41 %.

One may notice that these maps, w_1, w_2, and w_3, while satisfying the contractile initial conditions of Eqs. (2), operate in x over sub-intervals [0, 0.35], [0.35, 0.79], and [0.79, 1], and have vertical scaling parameters $d_1 = 0.18$, $d_2 = 0.30$, and $d_3 = -0.42$. As shown in Fig. 1, the iterations also induce intermittent projections dx and dy, over x and y, respectively, the first being a deterministic multinomial multifractal measure and the second the derived measure of such a dx via the fractal wire f, i.e., $dy = f^{-1}(dx)$, obtained adding all "events" over x corresponding to crossings of a given value of y.

To recap, while dx may be interpreted as the *input* to a *system* as defined by the fractal function f, dy is hence the *output*, which then could be thought of as a *transformation* of a *multiplicative cascade*, hence giving rise to the FM terminology.

The notions herein represent a generalization of the description of turbulent dissipation as a random binomial multifractal (Meneveau and Sreenivasan 1987) and the definition of other intermittent sets as random realizations of Levy processes via universal multifractals (Lovejoy and Schertzer 1990). As mentioned earlier, the FM approach may be given a physical interpretation as a realization of a non-trivial cascade process (Cortis et al. 2013), and then the patterns such as dy in Fig. 1 represent not only suitable geometric shapes but also sensible physical entities with which to represent natural phenomena.

As shown in Fig. 1, adjacent to dy, there are two other graphs named dy_h and dy_v that exhibit similarities with dy, but that contain distinct and additional zero values when seen from the y (time) axis. Such graphs do resemble the intermittencies of rainfall, including high peaks and the number of zeros, and are defined as follows. On the one hand, dy_h is found by considering a horizontal threshold, ϕ_h, as shown on the input dx, and transforming only the mass above it via the same function f. Such a derived measure (shown normalized so that its total mass is one unit) may then be interpreted as the output produced by sufficiently large eddies (in x), as it happens when rainfall is formed aided by turbulence. The set dy_v, on the other hand and shown on the far right, is obtained by using a vertical threshold, as depicted on the output dy, and normalizing the total mass to one, as is customarily done in practice when "traces" of rainfall less than a cutoff, and in consonance with the inherent accuracy of the measurements, are neglected.

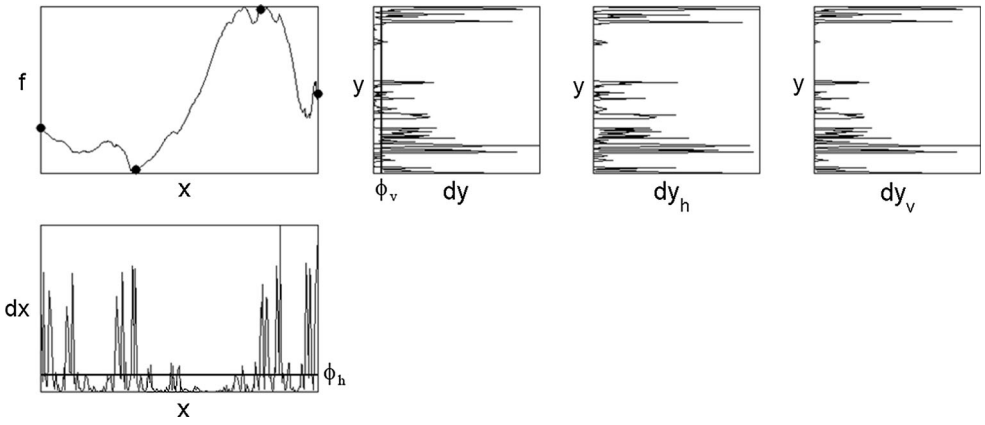

Fig. 1 The original FM approach: from an multinomial multifractal dx, to a derived projection dy, via a fractal interpolating function from x to y, followed by two adaptations: a projection dy_h, found pruning dx below a horizontal threshold ϕ_h, and a projection dy_v found pruning dy below a vertical threshold ϕ_v

Both kinds of sets dy_h and dy_v represent the adaptations of the FM approach that shall be used later on in order to model complex rainfall records gathered at the daily scale. This implies solving an inverse problem for a given set that includes as parameters: (a) the interpolating points by which a fractal interpolating function passes; (b) the vertical scalings d_n; (c) the frequencies used on each map in chaos game calculations; and (d) a horizontal or vertical threshold for a total of 7 and 11 parameters, respectively, for representations based on two and three affine maps. It ought to be noted that, as dx and dy are found as histograms of all chaos game points, dy_v is more easily computed than dy_h, for the latter requires pruning the chaos game and, hence, is a more expensive procedure.

2.2 An extension of the FM method to Cantorian inputs

Instead of using a wire defining a fractal interpolating function, the affine maps may be modified so that they define a more general attractor containing holes of different sizes, as present in Cantorian measures (Mandelbrot 1982). Such may be done using N maps as in Eq. (1), but using new contractile initial conditions,

$$w_n\begin{pmatrix}x_0\\y_0\end{pmatrix}=\begin{pmatrix}x_{2n}\\y_{2n}\end{pmatrix},\quad w_n\begin{pmatrix}x_{2N-1}\\y_{2N-1}\end{pmatrix}=\begin{pmatrix}x_{2n+1}\\y_{2n+1}\end{pmatrix},\quad n=1,\ldots,N, \tag{6}$$

such that the domain of map w_n becomes the interval $[x_{2n}, x_{2n+1}]$. Notwithstanding the need of additional end-point parameters y_{2n}, y_{2n+1}, a Cantorian measure is obtained whenever the domain maps define gaps (Huang et al. 2013).

Figure 2 shows an example of this extension for an attractor passing by the two sets of end-points $\{(0,0),(0.39,-1.54)\}$ and $\{(0.77,-5.0),(1,1)\}$, marked by the circles, and corresponding to the two affine maps

$$w_1\begin{pmatrix}x\\y\end{pmatrix}=\begin{pmatrix}0.39 & 0\\-1.82 & 0.28\end{pmatrix}\begin{pmatrix}x\\y\end{pmatrix} \tag{7}$$

$$w_2\begin{pmatrix}x\\y\end{pmatrix}=\begin{pmatrix}0.23 & 0\\6.47 & -0.47\end{pmatrix}\begin{pmatrix}x\\y\end{pmatrix}+\begin{pmatrix}0.77\\-5.00\end{pmatrix} \tag{8}$$

iterated according to proportions 66 and 34 %.

Upon 2^{14} successive iterations of these maps, the shown Cantorian attractor (x vs. y) is found, which induces projections dx and dy, the first one clearly defined over a Cantor set with the largest hole from 0.39 to 0.77 (a gap of 0.38 between the two maps) and with the second one, the derived distribution over y, exhibiting holes, but not arranged in a repetitive fashion as dx.

As in Fig. 1, adjacent to the derived measure over y in Fig. 2, there are two additional patterns named dy_h and dy_v, which correspond to further refinements either by a horizontal threshold on the input measure dx or by a vertical threshold of dy itself that yields additional zero values.

As with the original FM approach, both kinds of patterns dy_h and dy_v adapted from Cantorian inputs shall be used to model complex rainfall records. This implies solving a slightly more involved inverse problem that includes as optimizing parameters: (a) the end-points that define a more general attractor containing holes; (b) the vertical scalings d_n; (c) the frequencies used on each map in chaos game calculations; and (d) a horizontal or vertical threshold for a total of 9 and 15 parameters, respectively, for representations based on two and three affine maps. As before, dy_v is more easily computed than dy_h, for the latter requires pruning the chaos game.

3 Strategy for inverse problem and suitable statistics

Even though the notions presented above are easy to implement and projections are computed rather quickly once a set of parameters is known, there are non-trivial

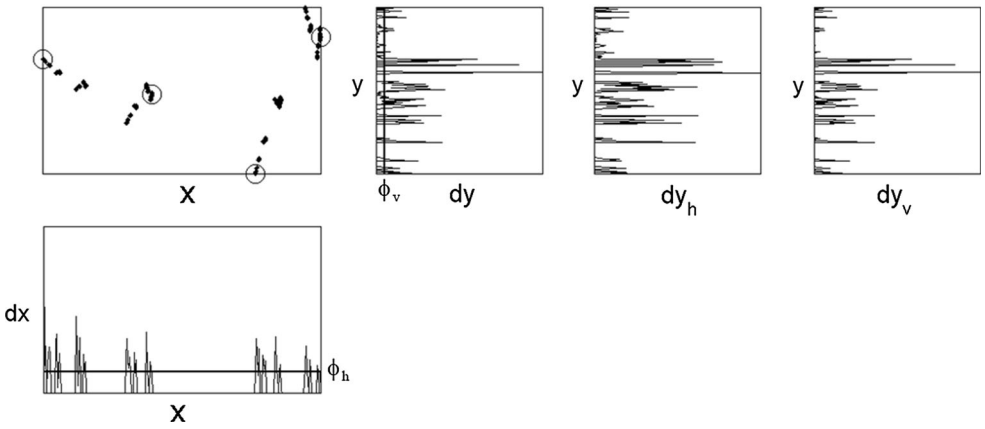

Fig. 2 A generalized FM approach: from a Cantorian texture dx, to a projection dy, via a disperse attractor from x to y, followed by two adaptations: a projection dy_h, found pruning dx below a horizontal threshold ϕ_h, and a projection dy_v found pruning dy below a vertical threshold ϕ_v

challenges in solving an inverse problem, finding suitable parameters for a given data set. To start, there are no analytical expressions available for the derived measures in terms of the FM parameters and, hence, a numerical search, in a space having high dimensionality, is required. This is realized, for instance, by noticing that, as just mentioned, there are 9 and 15 parameters needed when using the Cantorian extension with two and three maps, respectively. In addition, the inverse problem is complex, as results also depend on the definition of the objective function and the optimization algorithm used (Huang et al. 2013) and as, not surprisingly, alternative searches lead to non-unique solutions and trappings into local minima (Hill and Tiedeman 2007).

Following the success in encoding continuous rainfall events gathered at a very fine scale, i.e., seconds, and for a few hours (Huang et al. 2013), here we report the results found using a generalized particle swarm optimization (GPSO) algorithm in order to attempt solving the inverse problem involved. Inspired by the collective social behavior of animals (Kennedy and Eberhart 1995), such heuristic PSO algorithms that follow a "leader" have been extensively used in complex optimization processes. Specifically, we adopt here a "cloud" version of the PSO algorithm in which all members of the swarm interact with one another, hence providing additional dynamic capabilities (Fernández Martínez et al. 2010). In addition, and as the search happens over high-dimensional parameter space, we start the search at 100 FM parameter values obtained randomly and then allow swarms containing 300 members each to evolve towards a plausible solution. At the end, the best of the 100 cases, even if a local optimum, is considered as a "suitable solution."

In regards to the objective function, and based on our experience (Obregón et al. 2002a, b; Huang et al. 2013), we consider basically the L^2 norm (i.e. the root mean square error) of accumulated measured rainfall versus accumulated FM fitted values over the period of consideration, referred as, *RMSEAR*:

$$RMSEAR = \sqrt{\frac{1}{M}\sum_{i=1}^{M}(r_i - \hat{r}_i)^2} \tag{9}$$

where M is the number of data points, r_i is the accumulated measured rainfall up to day i and $\hat{r}_i$ is the accumulated FM-fitted rainfall up to day i.

Attempting to ensure that FM solutions shared similar geometrical features with the target set, various penalties are added to the aforementioned objective function. Such include: (a) the maximum deviations between measured and FM fitted records (MAXEAR), which could not exceed on any given day a value of 10 %; (b) the length of the FM data set, from beginning to end, which should be within 10 % of the target set; and (c) the number of zeros in the FM fit, or no-rain events, which should be within 5 % of those for the target set. These penalties are implemented adding such terms to the objective function employing various weights. Although the calculations via the PSO method may not always keep those restrictions all the time, the results, to be presented in the next section, are found to ultimately achieve all such constraints.

In order to qualify the goodness of the obtained FM sets, various statistics, not included in the optimization exercise, are computed. Such include comparisons between key features of normalized observed and fitted sets (so that they integrate to 1), that comprise the autocorrelation functions, the data's histogram, and their Renyi entropy function defined by

$$H(q) = \frac{1}{1-q}\log\left(\sum_{i=1}^{M} p_i^q\right), \tag{10}$$

where p_i is the precipitation (observed or fitted) at day i and q is an exponent weight that varies in this study from 0.1 to 5.1. To do the comparisons, the well-known concept of the

Nash–Sutcliffe efficiency (Nash and Sutcliffe 1970) is considered,

$$NSE = 1 - \frac{\sum_{i=1}^{S}(r_i - \hat{r}_i)^2}{\sum_{i=1}^{S}(r_i - \bar{r})^2}, \quad (11)$$

where r_i is the ith statistical value for observed data set, $\bar{r}$ is the mean of such a statistic over the total number of statistics considered S, and $\hat{r}_i$ is the ith statistical value for an FM fit.

4 Encoding rainfall records

The applicability of the FM approaches reviewed in Sects. 2.1 and 2.2 is reported next for four sets of typical daily rainfall records: two gathered in Laikakota, Bolivia and two measured in Tinkham, Washington, USA. While the Laikakota sets (provided by Ministerio de Medio Ambiente y Agua, Bolivia) span the 1965–1966 and 1966–1967 water years (from October 1st to June 30th, for a total of 273 consecutive days), the Tinkham observations (National Resource Conservation Service, Station ID 899) correspond to the 1993–1994 and 1994–1995 water years (whole years of 365 observations starting October 1st). In the case of Laikakota data sets, only 273 days are considered because the records show there is no major activity for the rest of the year. Prior to attempting fitting the given sets, the data are normalized so that the accumulated volume becomes a unity.

Given the geometric intricacies present in the records, FM representations based on two and three affine maps are considered. As such, the results presented below correspond to encodings having 7 and 9 parameters when using fractal wires, and 9 and 15 parameters when employing Cantorian attractors, respectively, for FM approaches based on two and three maps. As a consequence, the results correspond to encodings with compression ratios that are at least 18:1 for the Laikakota sets (273/15) and 24:1 for the Tinkham sets. As the optimization exercise for trying to solve the inverse problem for a given set is quite involved, we present not only the "best" results for the objective function considered but also two other approximations in distinct regions of the FM parameter space. This will certainly help to appreciate the overall suitability of the FM approach, not only as an encoding algorithm but also as a procedure to define relevant simulations of natural intermittent sets.

4.1 FM representations for data sets in Laikakota, Bolivia

Figure 3 portrays, on the top left, the measured data set for the water year 1965–1966 and, on the top right, the corresponding accumulated rainfall over the period. As may be seen, this rainfall set exhibits noticeable intermittency, as reflected by three major peaks and at least six notorious intervals of no rain and by a rough accumulated rain set that stays below the line of average rain for roughly 40 % of the time.

Figure 3 also contains three distinct FM approximations for the daily rainfall records (A–C), and their accumulated sets overlaid by the observed accumulated rain, found from Cantorian representations and the notion of vertical thresholds, as explained in Fig. 2. While the ones labeled A and C use an FM model with three maps, B employs an FM model based only on two maps. The actual values of the parameters for such sets are included in Appendix 1.

As may be readily seen, all representations are excellent in their ability to approximate the accumulated target and have root mean square errors in accumulated rainfall (RMSEAR) that are less than a mere 1.8 % and maximum errors in accumulated rain (MAXEAR) that do not exceed 5 %, with the set labeled B having a rather small value of 3.5 % for such an attribute. Although the FM representations are not capable of capturing all three noticeable peaks on the records, but only two at most, all representations do capture the most massive peak, as seen in the steepest section of the accumulated rain profile. Altogether, the three FM sets do share similar textures as does the original one and they may not be taken apart from one another. This is the case as even the shown horizontal dashed lines, indicating that below them lies 90 % of the mass, are quite close to one another and to that of the original set.

Figure 4 and Table 1 include further statistical information that corroborates the goodness of the fits and the fact that the sets do have comparable "textures." Figure 4 includes plots of the histogram, Renyi entropy, and autocorrelation function of the records, when compared to those of the data. As readily seen, the FM histograms for all cases—built with 10 intervals from minimum to maximum of actual records (set to one)—approximate very well the one for the observed records, which contains a sizable amount of mass for values close to zero. This is reflected by the close-to-one values for the Nash–Sutcliffe statistic for the histogram of rain (NSHR) as seen on the second column of Table 1, and close locations of the vertical dashed lines in Fig. 4 at a 90 % level—the equivalent of the horizontal dashed lines in Fig. 3—as indicated by the percent histogram mass in fitted records corresponding to 90 % in observed data (PF90) (Table 1, third column). Although the histogram is well fitted by all FM representations, this does not mean that the actual timing of, say, zero values is equally well matched as well. Nevertheless, the percent of time such do match is quite high (above 70 %) (see the column PZMR in Table 1).

Although the "textures" of the FM fittings and records appear to be comparable by the eye, such may indeed be

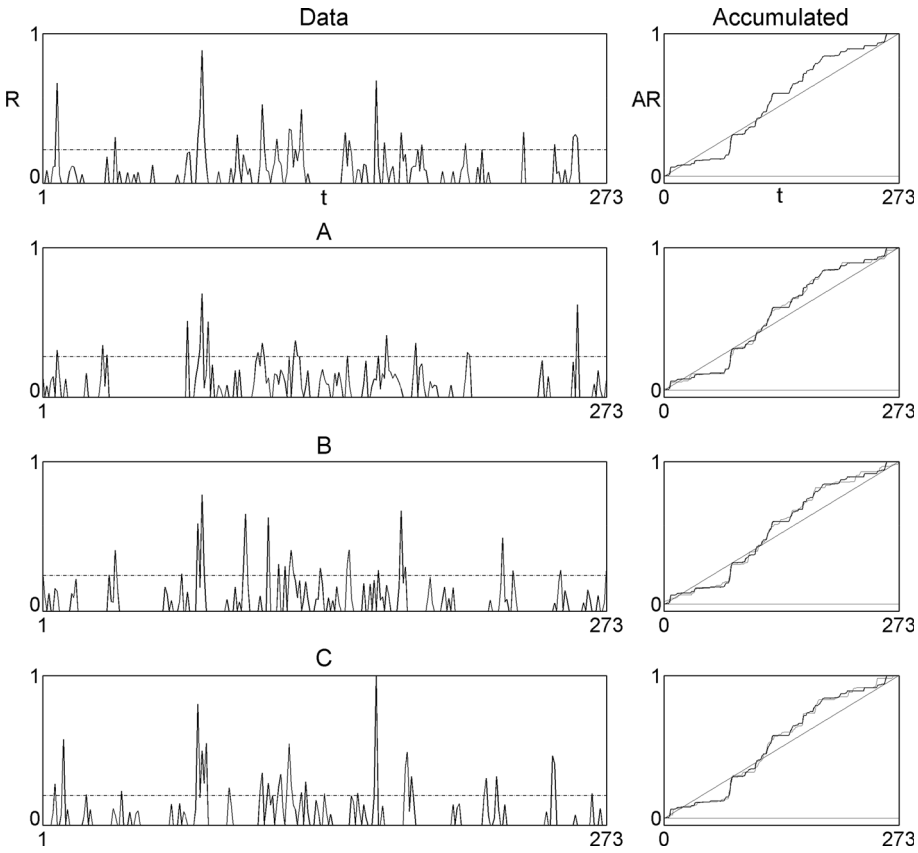

Fig. 3 Measured rainfall records in Laikakota, Bolivia gathered daily from September 1965 to May 1966 and three suitable FM fittings (**A**–**C**) followed by their accumulated sets. The root mean square error and maximum error in cumulative sets (RMSEAR, MAXEAR) are, in order, 1.4 and 4.4 % for **A**; 1.8 and 3.5 % for **B**; and 1.7 and 5.0 % for **C**

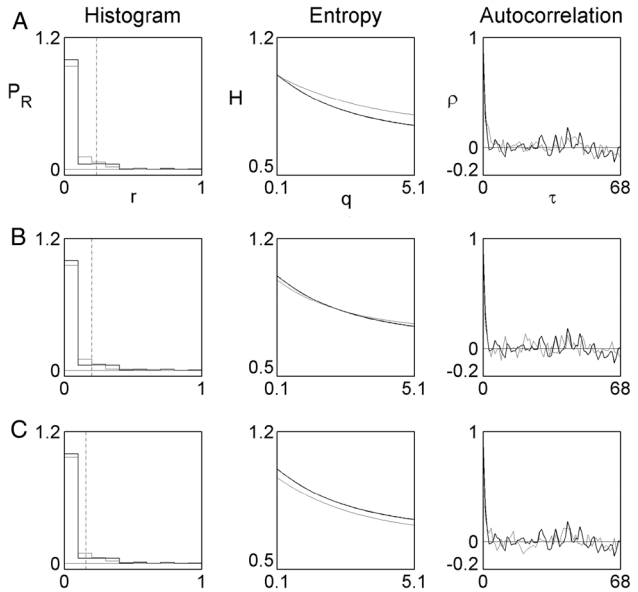

Fig. 4 Graphical representation of statistics of three FM fits shown in Fig. 3 in terms of histogram, entropy and autocorrelation. Observed data is plotted in *black* and FM model in *gray*

tested by calculating the Renyi entropy, say, from 0.1 to 5.1 in increments of 0.1 for a total of 51 values, and comparing the results. As seen in Fig. 4 (second column), the entropy of set labeled B closely follows that of the original data, with set A being the worst in capturing such an attribute. At the end, the Nash–Sutcliffe statistic for entropy (column NSER in Table 1) reflects the nature of the fitted textures, with models B and C being superior.

The last column of Fig. 4 includes the autocorrelation function of the FM models and of the records. As seen, such correlations—spanning 68 days—decay rather quickly and, while remaining close to zero, become statistically insignificant. As included in Table 1, the lag at which the autocorrelation reaches zero for the first time (AL0) happens for the data at 3 days, while FM models B and C follow closely. As may be expected, given their insignificant nature, the Nash–Sutcliffe comparison regarding autocorrelations (seen in Table 1 as NSACR) yields poor fittings reflected by negative values, indicating more variability in comparing sets that in the intrinsic variance of the record's autocorrelations.

Figures 5 and 6 show (similarly to Figs. 3 and 4) the results for the rainfall records in Laikakota, for the water year 1966–1967. As seen in the top of Fig. 5, this set also exhibits noticeable intermittency as reflected by two major peaks and eight notorious intervals of no rain and also possesses a rough accumulated rain set that comes close to or crosses the line of average rain at four intermediate times.

Table 1 Error statistics associated with Fig. 3

Fits	NSHR (%)	PF90 (%)	PZMR (%)	NSER (%)	AL0	NSCAR (%)
A	99.5	92.6	72.4	66.8	3(8)	−8.3
B	99.6	90.8	71.8	98.2	3(4)	−69.5
C	99.9	88.6	77.0	82.5	3(5)	−30.0

The three distinct FM approximations of such a set, shown in Fig. 5, also come, as before, from Cantorian representations and the notion of vertical thresholds, as explained in Fig. 2. While the actual parameters for such sets are included in Appendix 1, the one labeled A uses an FM model with two maps and the sets B and C employ the FM approach based on three maps. As may be appreciated, all representations shown for this set are excellent, as they approximate the accumulated target closely, with RMSEAR values less than just 1.9 % and with MAXEAR values less than 6.5 %. Observe that although the FM models cannot preserve the two noticeable peaks, but only one, all representations again do very well capture the accumulated rain profile and the overall texture of the original records.

As seen in Fig. 6 and Table 2, the FM fits do represent suitable alternatives for modeling the original set. The histograms for all cases approximate very closely the one for the observations, which, as before, contain many values close to zero and have their 90 % levels (PF90) very close to one another—as also seen in the horizontal dashed lines in Fig. 5. Regarding the percent of zero values matched, these FM representations turn out to be a bit better than those for the previous water year, as all values exceed 74 % (see PMZR in Table 2).

In relation to the nature of the textures, it may be seen that the best fit regarding the objective function (A) does not correspond to the best fit in Renyi entropy (B). As found earlier for the 1965–1966 year record from Laikakota, Nash–Sutcliffe values for such an attribute (NSER in Table 2) are quite high, with models B and C, having inferior objective functions, being superior here. Altogether, however, all FM representations appear feasible to the naked eye.

Finally, the autocorrelation functions for the data and FM models decay rather fast for this set (see Fig. 6, last column, and Table 2, last two columns). While the records reach a zero correlation on only 2 days, the models follow

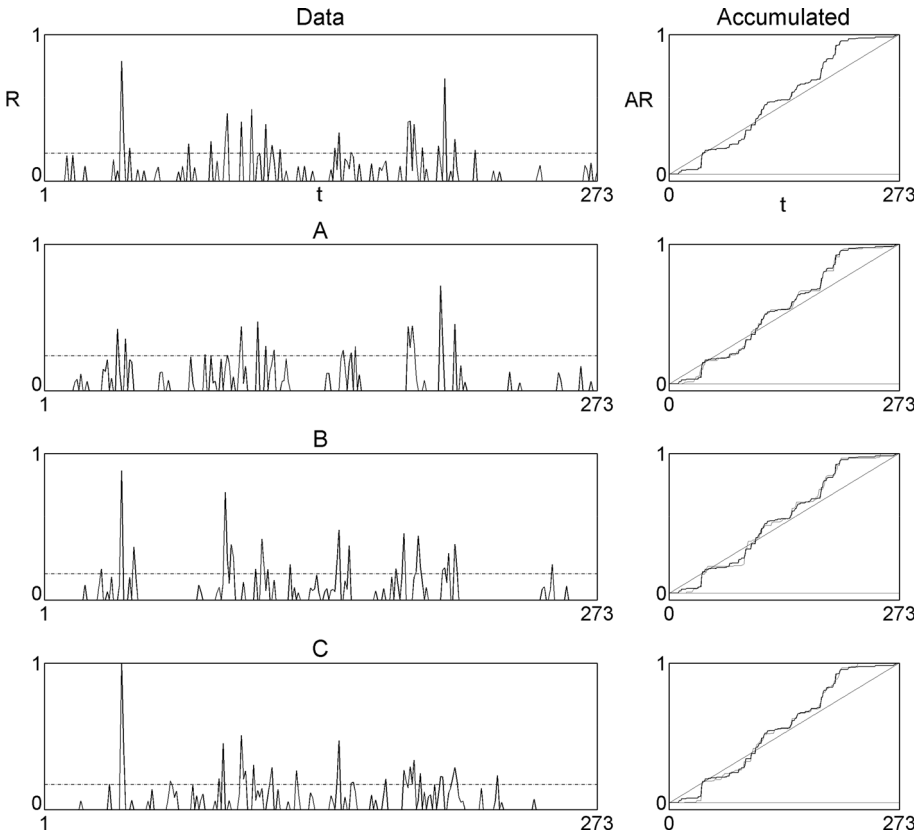

Fig. 5 Measured rainfall records in Laikakota, Bolivia gathered daily from September 1966 to May 1967 and three suitable FM fittings (**A**–**C**) followed by their accumulated sets The root mean square error and maximum error in cumulative sets (RMSEAR, MAXEAR) are, in order, 1.4 and 5.7 % for **A**; 1.9 and 6.4 % for **B**; and 1.7 and 4.6 % for **C**

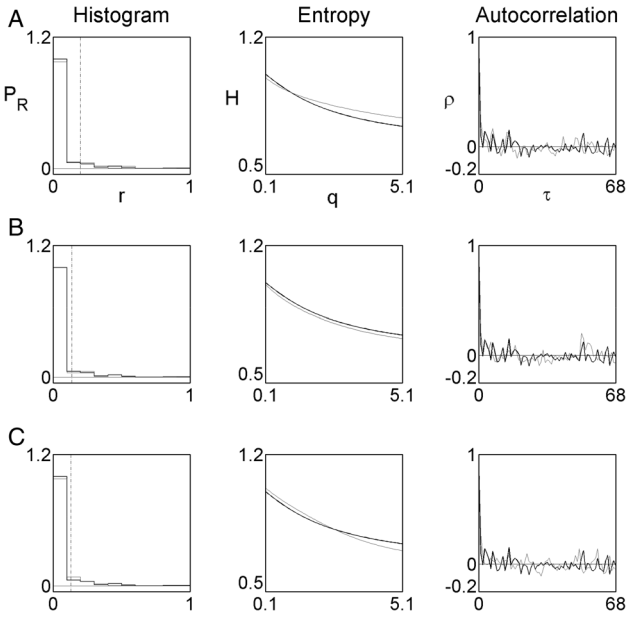

Fig. 6 Graphical representation of statistics of three FM fits shown in Fig. 5 in terms of histogram, entropy and autocorrelation. Observed data is plotted in *black* and FM model in *gray*

closely, with the one labeled B being the worst, although it has the best entropy. As before, the Nash–Sutcliffe values (NSACR in Table 2) reflect the quick decay to statistically insignificant values, and hence the three FM representations may be deemed good in all qualifiers considered.

4.2 FM representations for data sets from Tinkham, Washington

Figures 7 and 8 show the data sets (top) and three FM fits, as found for the two data sets considered in Tinkham during 1993–1994 and 1994–1995 for the whole year of 365 days. As seen (top), these sets appear to be "more complex" than the ones from Laikakota, Bolivia. As reflected by several major peaks, these sets exhibit even more noticeable intermittency, even if they contain about the same number (seven) of notorious intervals of no rain. As seen, both sets have rough accumulated rain profiles that remain above the line of average rain most of the time.

As found for the Laikakota sets, the three distinct FM approximations portrayed on each figure are based on the notion of vertical thresholds. All of them employ three maps, and their parameters are included in Appendix 1. As may be readily appreciated, all representations shown for these rather complex sets are also excellent, as they yield close renderings of the accumulated sets. For instance, the RMSEAR values are less than just 1.7 % and the MAXEAR values are less than 6.1 %; however, at least one FM fit has a mere 1.1 % in the objective function (A on both years). Further, it can be noticed that there is a rather low maximum error in accumulated rain of 2.7 and 4.1 % (for fit B in Fig. 7 and for fit C in Fig. 8). Notice how the FM models do capture the accumulated rain profile very well and also the overall "appearance" of the original records.

Tables 3 and 4 include some of the statistics already reported for the histogram, entropy, and autocorrelation functions of the records when compared with the FM fits (The counterparts of Figs. 4 and 6 are not presented here, as they look almost identical to the ones for the Laikakota sets). In regards to the histograms, the second column of Tables 3 and 4 reflect a rather close agreement of observed versus FM fitted sets, with all Nash–Sutcliffe values (NSHR) being quite close to 1. As found before for Laikakota, the 90 % level for the accumulated mass—the dashed horizontal lines in Figs. 7 and 8—are well preserved (see column PF90 in Tables 3 and 4) and there is also good matching of zero values, which remains above 71 %.

Regarding the entropies, the FM models for Tinkham data turn out to be even better than the ones for Laikakota, as reflected by the NSER values that are higher than 91 % except for the model labeled C in Fig. 8 which has a high number (71 %). And, finally, in regards to autocorrelations, the FM sets closely follow the first lag to zero correlation (AL0), which is now about 12 days, and, perhaps a bit surprisingly, the Nash–Sutcliffe for autocorrelations for the year 1993–1994 in Fig. 7 are much better than the one for the other year 1994–1995, which otherwise is comparable to what was reported for the Laikakota sets.

Altogether, the FM representations in Figs. 7 and 8 provide suitable approximations to the 2 years considered, although it ought to be emphasized that these sets are more difficult to encode than the ones from Laikakota, which exhibit a slightly lower level of complexity.

4.3 Summary of encodings

For all the four rainfall data sets studied in detail here, it may be said that: (a) though most of the records require

Table 2 Error statistics associated with Fig. 5

Fits	NSHR (%)	PF90 (%)	PZMR (%)	NSER (%)	AL0	NSCAR (%)
A	100.0	92.6	79.2	83.9	2(5)	−24.3
B	100.0	89.4	78.2	95.7	2(8)	−0.6
C	99.8	89.0	74.8	92.8	2(4)	−67.3

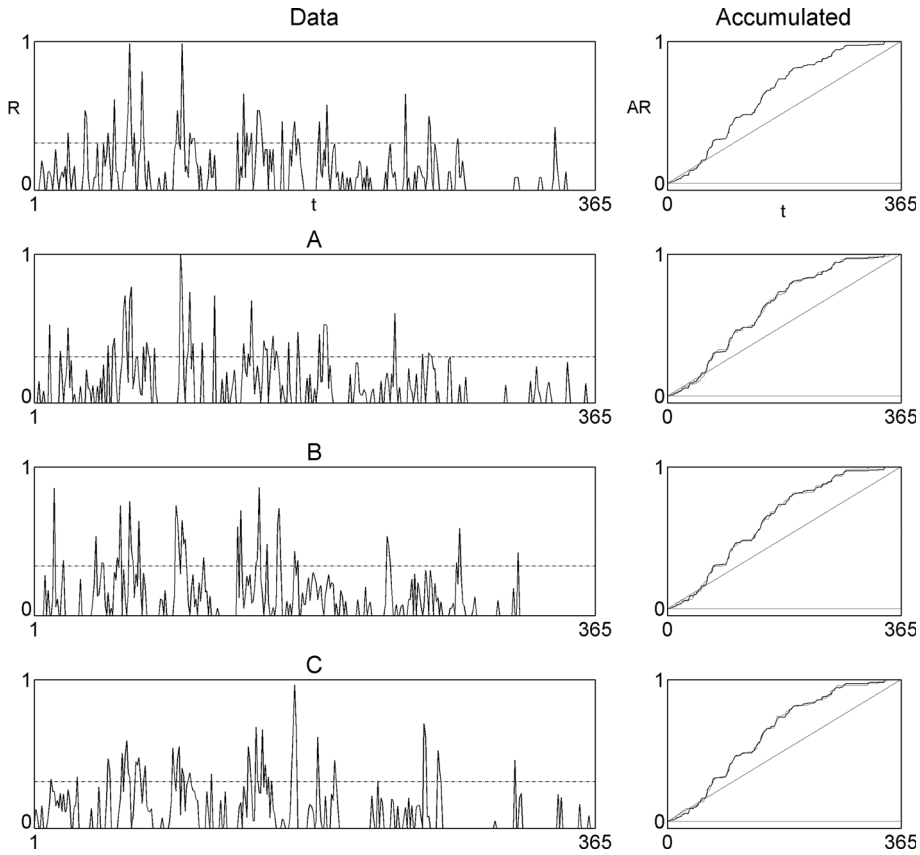

Fig. 7 Measured rainfall records in Tinkham, Washington gathered daily from September 1993 to October 1994 and three suitable FM fittings (**A**–**C**) followed by their accumulated sets. The average square error and maximum error in cumulative sets (RMSEAR, MAXEAR) are, in order, 1.1 and 3.1 % for **A**; 1.2 and 2.7 % for **B**; and 1.2 and 3.9 % for **C**

three maps to find the attractors via Cantorian inputs, two maps are sufficient in some cases to get reasonable results via Cantorian FM representations; (b) out of the twelve FM encodings presented, only one is found via a fractal wire and the original FM approach; (c) altogether, Cantorian representations with 15 FM parameters are found to be appropriate for the four data sets, leading to sizable compression ratios; (d) no cases are selected based on the more computationally expensive use of horizontal thresholds, as their errors are found to be a bit higher than those presented; and (e) there are several other FM parameter combinations that give similar statistical accuracy than the ones shown in the figures, which include best overall results in the objective function (RMSEAR), minimum value of maximum error in accumulated records (MAXEAR), and best fittings according to the entropy of the records (NSER). This final finding stresses the fact that there is non-uniqueness of the inverse problem, as expected.

5 Encoding twenty years of rainfall in Laikakota

Having illustrated in the previous section that the modified FM approach produces reasonable encodings of rainfall sets observed in both Laikakota and Tinkham, for a year at a time at the daily scale, it becomes interesting to study the effectiveness of the approach over a much longer period of data. Such is attempted here by applying the modified Cantorian FM method to 20 years (1963–1984) of rainfall observed at Laikakota, using two affine maps and a vertical threshold (i.e., as in Fig. 2). Each water year, starting in 1964–1965 and ending in 1983–1984, is encoded, as before, while selecting only one "best" solution having low RMSEAR and MAXEAR values.

Figure 9 presents the observed records (top) and FM fits (bottom) (upgraded to 365 days of non-normalized values having the same volumes as the observed records) of the 20-year Laikakota rainfall, and Fig. 10 shows the overall accumulated sets over the same period. As may be seen on each small section (i.e., year) (with the second and third FM fits corresponding to Figs. 3B and 5A), all years are closely approximated via FM representations that have similar appearances when compared to the measured sets. This is reflected by truly small RMSEAR values, whose magnitudes range from 1.3 to 2.2 % and have a mean and a standard deviation (over the 20 years) of 1.8 and 0.3 %, respectively; and by MAXEAR quantities, whose values span 3.5–8.8 % and have mean and standard deviation values of 5.6 and 1.3 %, respectively. Altogether, the FM representation of the 20-year rain turns out to be excellent,

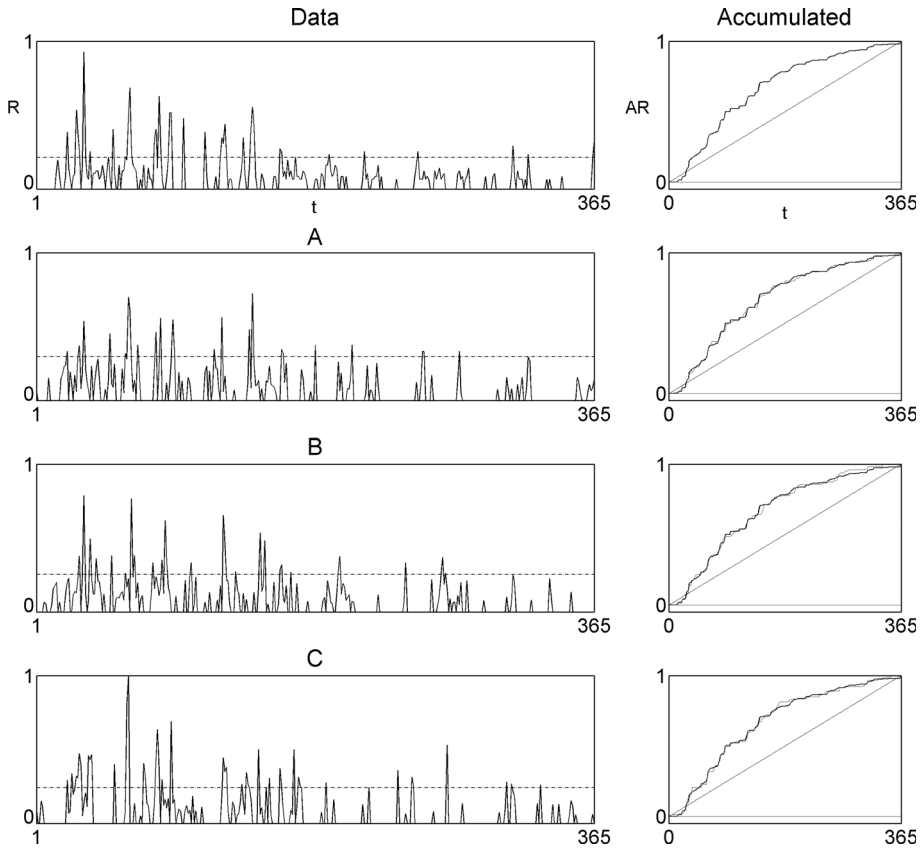

Fig. 8 Measured rainfall records in Tinkham, Washington gathered daily from September 1994 to October 1995 and three suitable FM fittings (**A**–**C**) followed by their accumulated sets. The average square error and maximum error in cumulative sets (RMSEAR, MAXEAR) are, in order, 1.1 and 4.4 % for **A**; 1.7 and 6.1 % for **B**; and 1.4 and 4.1 % for **C**

Table 3 Error statistics associated with Fig. 7

Fits	NSHR (%)	PF90 (%)	PZMR (%)	NSER (%)	AL0	NSCAR (%)
A	99.9	89.5	71.9	96.8	12(9)	44.8
B	99.7	91.3	71.9	96.8	12(16)	34.9
C	99.4	89.8	74.9	94.8	12(13)	57.2

Table 4 Error statistics associated with Fig. 8

Fits	NSHR (%)	PF90 (%)	PZMR (%)	NSER (%)	AL0	NSCAR (%)
A	99.5	93.4	74.2	91.0	13(7)	16.2
B	99.4	92.3	72.2	96.2	13(12)	−70.7
C	99.8	91.9	73.7	71.3	13(13)	−29.5

as the overall deviations in the accumulated records in Fig. 10 (there are two accumulated records shown there) are a mere 0.081 and 0.65 % for RMSEAR and MAXEAR, respectively.

Figures 11 and 12, including, respectively, (a) the Renyi entropy function and two histograms (including and excluding zero values); and (b) various histograms of inter-arrival times of the 20-year records, further corroborate that the modified FM approach may indeed be useful in encoding rainfall in a practical setting. Notice the excellent agreements in Fig. 11, for both histograms and, in particular, the entropy, and the close following by the FM method of the histograms of inter-arrival times in Fig. 12, computed for six thresholds and limited to a lag of 50 days that accounts for the majority of the cases. These fits are certainly a welcomed feature, as they strongly suggest that the modified FM methodology may be useful not only to encode but also to simulate intermittent rainfall records.

At the end, the FM parameters shown in Fig. 13, as a function of time, turn out to reflect the evolution of the rainfall dynamics for the 20 years in Bolivia. The

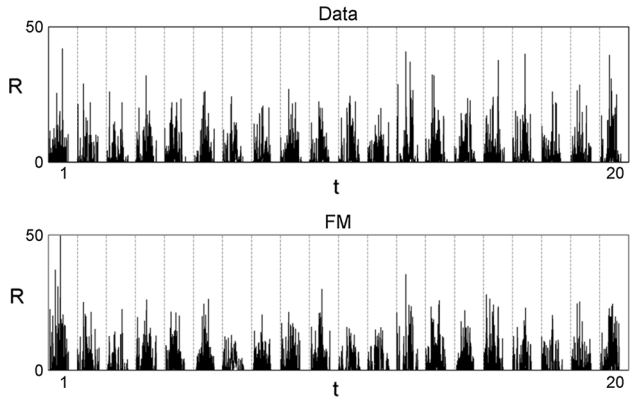

Fig. 9 Measured rainfall gathered in Laikakota, Bolivia from water year 1964–1965 until 1983–1984 and corresponding FM representations (year by year) based on two maps and the adaptation based on a vertical threshold

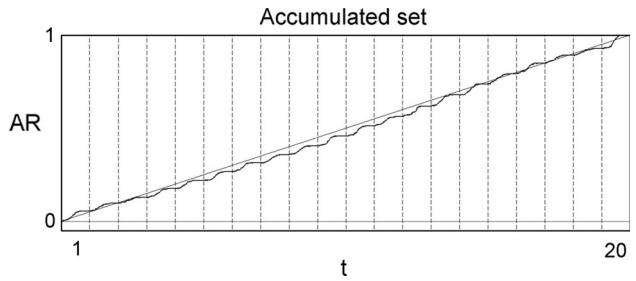

Fig. 10 Accumulated rainfall sets corresponding to measured rainfall and FM representations in Fig. 9

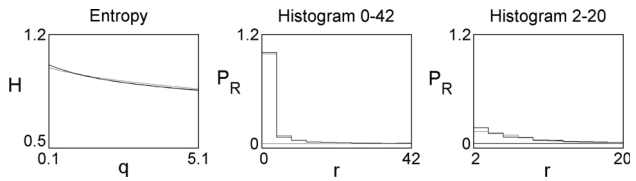

Fig. 11 Renyi entropy function followed by two rainfall histograms, from 0 to 42 (mm) and 2 to 20 (mm), corresponding to the measured rainfall and FM representations in Fig. 9. The number of events (days) considered on the histogram from 0 to 42 is 7300, and the FM values beyond 42 mm is placed on the last of 10 bins. The number of events (days) considered on the sub-histogram from 2 to 20 are 1248 for data and 1287 for FM fit. Observed data is plotted in *black* and FM model in *gray*. The histograms are shown normalized so that the largest bin value is one

noticeable variability in parameters reflects the varied geometries from year to year, as seen in Fig. 9. That the evolution of only nine parameters may capture the evolving dynamics is certainly a desired feature, for such also suggests (even if trends may not be discerned that may allow predicting rainfall 1 year ahead) that such information may be useful in defining, via the swings in parameters, the intrinsic "complexity" of rainfall sets. It is envisioned that such variability in successive FM parameters may be used

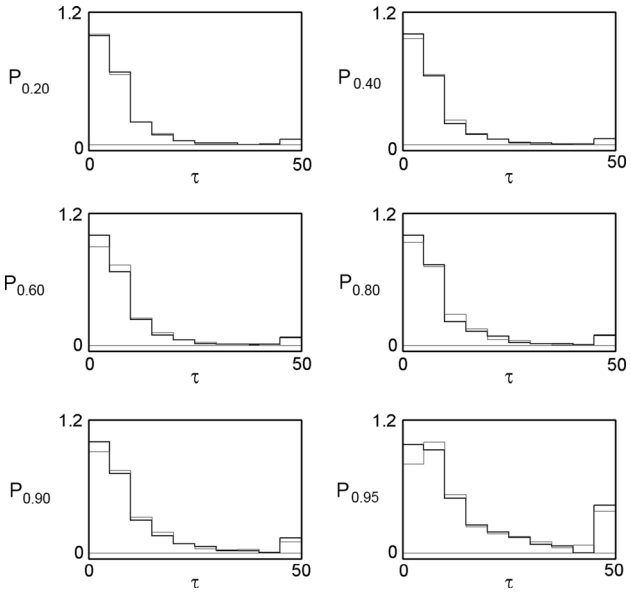

Fig. 12 Histograms of inter-arrival times for six thresholds corresponding to rainfall values associated with 20, 40, 60, 80, 90 and 95 % of the accumulated mass. So that differences may be discerned, all histograms are limited from 0 to 50 (days). All values beyond 50 days are placed on the last of 10 bins. The number of events considered, for measured and FM fits (in *parenthesis*), are from 20 to 95 %, in order, 809 (780), 748 (725), 671 (666), 599 (622), 507 (532), 284 (282). Observed data is plotted in *black* and FM model in *gray*. The largest bin value is normalized to one

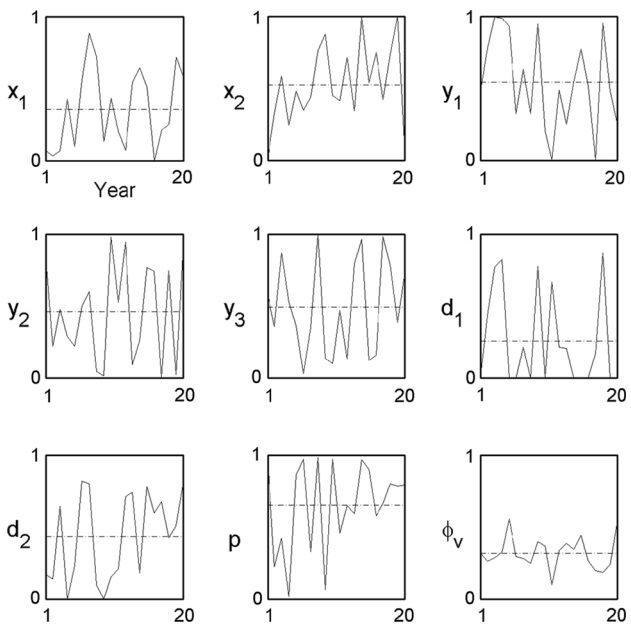

Fig. 13 FM parameters for the geometric representations of rainfall in Bolivia as shown in Fig. 9. The shown *dash lines* corresponding to mean values are, from *left to right* and *top to bottom*, 0.38, 0.53, 0.53, 0.45, 0.52, 0.22, 0.45, 0.65, and 0.31

to compare the complexity of rainfall records at various sites and that such may also help discern differences between previous and current conditions (e.g., between

20 years in the past and 20 years ending in the present), in a way that may allow addressing issues related to climate change.

6 Concluding remarks

This study has illustrated how the FM approach (and its extensions) may be adapted, via thresholds, in order to encode daily rainfall data, especially those that are highly intermittent. Through a detailed study of four distinct rainfall data sets, two each from two different locations (Laikakota, Bolivia, and Tinkham, Washington, USA), and later via the use of 20 years of records in Laikakota, it has been illustrated, for the first time, that the deterministic geometric procedure, could possibly replace, and certainly enhance, existing stochastic procedures for representing the highly intermittent rainfall process, in a manner that hints at hidden determinism in natural complexity (Puente 1996; Puente and Sivakumar 2007). The present applications certainly suggest a novel way for representing the dynamic variations of complex rainfall (and also other hydrologic) records encountered at the daily scale, one that relies on a reduced geometric space of FM parameters.

As the FM representations obtained may be bounded by the usage of three affine maps leading to 15 geometric parameters, the results shown here yield compression ratios that are as high as 18:1 for the Laikakota data sets and as high as 24:1 for the sets from Tinkham. Although it may appear that the number of FM parameters is high when compared to the number of parameters commonly used in stochastic models, it ought to be emphasized that the latter—relying on statistical information, such as autocorrelations, power spectrum, and multifractal spectrum (co-dimension function)—cannot easily produce realizations that adequately capture the specific details of a given precipitation data set.

Even though the FM representations shown are remarkable in regards to the accumulated records, yielding in all cases almost perfect correlations between observed accumulated rain and FM fitted accumulated rain (r^2 in excess of 99 %), it ought to be realized that the actual rains themselves, although indistinguishable to the naked eye and statistically, are indeed distinct. As a consequence, calculation of the Nash–Sutcliffe qualifier for the rain sets themselves may be in several cases negative, as it happened, for instance, with the observed and FM fitted autocorrelation functions. This fact reflects the inherent complexity of the records and the imperfection of the FM fits. However, if records are aggregated to the weekly scale, there start to appear good agreements between the observed and FM fitted sets (results not shown here). In fact, calculation of the Nash–Sutcliffe coefficient for weekly rainfall (NSR7) gives for the four Figs. 3, 5, 7, and 9 and for the three FM approximations A–C, in order: 70.9, 36.4, 39.4 %; 54.6, 59.9, 77.8 %; 61.1, 52.1, 70.2 %; and 63.8, 45.4, 61.1 %, which implies that there are at least one FM fit per data set that exceeds 63.8 %, a rather good number in many geophysical applications.

To continue the discussion for rainfall data at the weekly scale, it ought to be repeated that suitable FM models, comparable in accuracy to those reported in Sect. 4, may also be found for data at such a scale. As accumulating at the daily scale and at the weekly scale match surely every 7 days, these FM representations based on weeks, when calculated at the daily scale, provide sensible approximations of the accumulated records. As a consequence, the FM approach may be downscaled to provide approximations of a given set, representations whose accuracy depends on the inter-weekly details but that closely approximate what happens every week. This is a welcomed feature of the FM approach, as a variety of downscaling representations may be obtained based on various FM representations.

The highly promising results explained herein, on a yearly basis and certainly when compounded over 20 years, further support the idea that complex rainfall patterns may be wholly understood in a deterministic fashion (Puente and Sivakumar 2007). Given the recent reports of precipitation measurements being plagued with non-trivial errors (Lanza and Vuerich 2009), it may also be argued that all representations herein, with maximum deviation from cumulative deviations (at the original resolution) of 1.8 % on the average over 20 years for Laikakota, are more than acceptable renderings of what nature produces. Whether the FM parameters allow predictions of years at a time and whether the FM parameters allow defining the complexity of records, with a potential application to climate change, are certainly interesting and relevant issues that shall be discussed elsewhere.

Acknowledgments The research leading to this article was supported by a JASTRO Award provided to the first author by the University of California, Davis. We are thankful to Ministerio de Medio Ambiente y Agua, Bolivia for providing rainfall records gathered at Laikakota and also to the team of National Resource Conservation Service for the availability of rainfall records in its web portal. Bellie Sivakumar acknowledges the financial support from the Australian Research Council (ARC) through the Future Fellowship grant awarded to him (FT110100328). The thoughtful comments from anonymous reviewers are gratefully acknowledged, as they resulted in an improved manuscript, both technically and in presentation. Those are gratefully acknowledged.

Appendix 1: FM parameters for rainfall encoding

Figure	Maps	X_1	X_2	X_3	X_4	Y_1	Y_2	Y_3	Y_4	Y_5	d_1	d_2	d_3	p_1 (%)	p_2 (%)	p_3 (%)	ϕ_v (%)
3A	3	0.525	0.704	0.390	0.907	−4.583	2.478	−1.907	1.185	−0.911	0.116	0.455	−0.573	24.4	25.5	50.1	30.8
3B	2	0.033	0.327	1	–	2.737	−2.758	−1.417	–	–	−0.136	−0.715	–	22.7	77.3	–	26.3
3C	3	0.367	0.630	0.443	0.958	1.578	0.575	−1.903	−2.002	1	−0.358	−0.250	0.128	43.8	17.7	38.5	16.1
5A	2	0.068	0.584	1	–	4.951	−0.249	3.709	–	–	0.536	0.288	–	42.3	57.7	–	28.7
5B	3	0.759	0.256	0.316	0.947	0.526	−2.137	1.222	−3.538	0	−0.692	0.127	−0.003	31.4	39.4	29.2	5.7
5C	3	0.000	0.613	0.271	0.374	4.992	2.287	−2.847	−1.669	5	0.143	0.173	0.010	43.0	32.4	24.6	3.3
7A	3	0.277	0.545	0.589	0.988	−2.688	−2.431	1.697	0.015	5	0.184	−0.374	−0.312	32.9	38.7	28.4	12.1
7B	3	0.117	0.463	0.149	0.385	4.643	2.531	0.798	−0.915	2.023	−0.316	−0.530	−0.255	43.2	20.5	36.3	19.9
7C	3	0.101	0.000	0.760	0.566	−0.756	−0.570	−2.026	−2.206	5	−0.590	−0.191	0.269	37.7	13.1	49.2	14.5
8A	3	0.379	0.996	0.802	0.482	4.023	−3.796	4.909	0.057	5	−0.737	−0.239	0.461	64.8	32.8	2.4	27.7
8B	3	0.428	0.434	1	–	−0.368	−3.998	3.577	–	–	−0.069	0.341	−0.325	25.2	30.7	44.1	10.3
8C	3	0.003	1.000	0.366	0.327	−5.000	4.861	0.635	−3.766	0	0.182	−0.456	0.116	25.2	44.5	30.3	16.1

The domain for all cases goes from 0 to 1, i.e., $\mathbf{X_0} = 0$, $\mathbf{X_3}$ or $\mathbf{X_5} = 0$. The first vertical value is always 0, i.e., $\mathbf{Y_0} = 0$

All the cases come from FM Cantorian representations except 8B that uses a FM wire passing through four interpolating points

References

Barnsley MF (1988) Fractals everywhere. Academic Press, San Diego

Cortis A, Puente CE, Sivakumar B (2009) Nonlinear extensions of a fractal–multifractal approach for environmental modeling. Stoch Environ Res Risk Assess 23(7):897–906

Cortis A, Puente CE, Sivakumar B (2010) Encoding hydrologic information via a fractal geometric approach and its extensions. Stoch Environ Res Risk Assess 24(5):625–632

Cortis A, Puente CE, Huang HH, Maskey ML, Sivakumar B, Obregón N (2013) A physical interpretation of the deterministic fractal–multifractal method as a realization of a generalized multiplicative cascade. Stoch Environ Res Risk Assess 28(6):1421–1429

Feder J (1988) Fractals. Plenum Press, New York

Fernández Martínez JL, García Gonzalo E, Fernández Álvarez JP, Kuzma HA, Menéndez Pérez CO (2010) PSO: a powerful algorithm to solve geophysical inverse problems: application to a 1D-DC resistivity case. J Appl Geophys 71(1):13–25

Gupta VK, Waymire E (1990) Multiscaling properties of spatial rainfall and river flow distributions. J Geophys Res 95(D3): 1999–2009

Hill MC, Tiedeman CR (2007) Effective groundwater model calibration: with analysis of data, sensitivities, predictions and uncertainty. John Wiley & Sons Inc, Hoboken

Huang HH, Puente CE, Cortis A, Sivakumar B (2012) Closing the loop with fractal interpolating functions for geophysical encoding. Fractals 20(3–4):261–270

Huang HH, Puente CE, Cortis A, Fernández Martínez JL (2013) An effective inversion strategy for fractal–multifractal encoding of a storm in Boston. J Hydrol 496:205–216

Jayawardena AW, Lai F (1994) Analysis and prediction of chaos in rainfall and stream flow time series. J Hydrol 153:23–52

Jin YH, Kawamura A, Jinno K, Berndtsson R (2005) Nonlinear multivariate analysis of SOI and local precipitation and temperature. Nonlinear Process Geophys 12:67–74

Jothiprakash V, Fathima TA (2013) Chaotic analysis of daily rainfall series in Koyna reservoir catchment area, India. Stoch Environ Res Risk Assess 27(6):1371–1381

Kennedy J, Eberhart RC (1995) Particle swarm optimization. Proceedings of the IEEE international joint conference on neural networks. IEEE Service Center, Piscataway, pp 1942–1948

Kim HS, Lee KH, Kyoung MS, Sivakumar B, Lee ET (2009) Measuring nonlinear dependence in hydrologic time series. Stoch Environ Res Risk Assess 23:907–916

Kumar P, Foufoula-Georgiou E (1993) A multicomponent decomposition of spatial rainfall fields. Segregation of large and small scale features using wavelet transform. Water Resour Res 29(8):2515–2532

Labat D (2008) Wavelet analysis of annual discharge records of the world's largest rivers. Adv Water Resour 31:109–117

Labat D, Ababou R, Mangin A (2000) Rainfall–runoff relations for karstic springs—part II: continuous wavelet and discrete orthogonal multiresolution analyses. J Hydrol 238:149–178

Lanza LG, Vuerich E (2009) The WMO field intercomparison of rain intensity gauges. Atmos Res 94(4):534–543

Lorenz EN (1963) Deterministic nonperiodic flow. J Atmos Sci 20:130–141

Lovejoy S, Schertzer D (1990) Multifractals, universality classes and satellite and radar measurements of cloud and rain fields. J Geophys Res 95(3):2021–2034

Lovejoy S, Schertzer D (2013) The weather and climate: emergent laws and multifractal cascades. Cambridge University Press, Cambridge

Mandelbrot BB (1982) The fractal geometry of nature. Freeman, San Francisco

Mandelbrot BB (1989) Multifractal measures especially for the geophysicist. In: Scholz CH, Mandelbrot MM (eds) Fractals in geophysics. Birkhanser Verlag, Basel, pp 1–42

Meneveau C, Sreenivasan KR (1987) Simple multifractal cascade model for fully developed turbulence. Phys Rev Lett 59:1424–1427

Mishra AK, Özger M, Singh VP (2011) Wet and dry spell analysis of global climate model-generated precipitation using power laws and wavelet transforms. Stoch Environ Res Risk Assess 25:517–535

Nash J, Sutcliffe JV (1970) River flow forecasting through conceptual models, part I—a discussion of principles. J Hydrol 10(3): 282–290

Niu J, Chen J (2010) Terrestrial hydrological features of the Pearl River basin in South China. J Hydro-Environ Res 4:279–288

Obregón N, Puente CE, Sivakumar B (2002a) Modeling high resolution rain rates via a deterministic fractal–multifractal approach. Fractals 10(3):387–394

Obregón N, Puente CE, Sivakumar B (2002b) A deterministic geometric representation of temporal rainfall. Sensitivity analysis for a storm in Boston. J Hydrol 269(3–4):224–235

Puente CE (1996) A new approach to hydrologic modelling: derived distribution revisited. J Hydrol 187:65–80

Puente CE, Obregón N (1996) A deterministic representation of temporal rainfall: result for a storm in Boston. Water Resour Res 32(9):2825–2839

Puente CE, Sivakumar B (2007) Modeling hydrologic complexity: a case for geometric determinism. Hydrol Earth Syst Sci 11: 721–724

Puente CE, Robayo O, Díaz MC, Sivakumar B (2001a) A fractal–multifractal approach to groundwater contamination. 1. Modeling conservative tracers at the Borden site. Stoch Environ Res Risk Assess 15(5):357–371

Puente CE, Robayo O, Sivakumar B (2001b) A fractal–multifractal approach to groundwater contamination. 2. Predicting conservative tracers at the Borden site. Stoch Environ Res Risk Assess 5(5):372–383

Rodriguez-Iturbe I (1986) Scale of fluctuation of rainfall models. Water Resour Res 22(9):15S–37S

Rodrıguez-Iturbe I, De Power FB, Sharifi MB, Georgakakos KP (1989) Chaos in rainfall. Water Resour Res 25(7):1667–1675

Sivakumar B (2000) Chaos theory in hydrology: important issues and interpretations. J Hydrol 227(1–4):1–20

Sivakumar B (2004) Chaos theory in geophysics: past, present and future. Chaos, Solitons Fractals 19(2):441–462

Sivakumar B (2009) Nonlinear dynamics and chaos in hydrologic systems: latest developments and a look forward. Stoch Environ Res Risk Assess 23:1027–1036

Sivakumar B, Singh VP (2012) Hydrologic system complexity and nonlinear dynamic concepts for a catchment classification framework. Hydrol Earth Syst Sci 16:4119–4131

Sivakumar B, Sorooshian S, Gupta HV, Gao X (2001) A chaotic approach to rainfall disaggregation. Water Resour Res 37(1): 61–72

Sivakumar B, Woldemeskel FM, Puente CE (2014) Nonlinear analysis of rainfall variability in Australia. Stoch Environ Res Risk Assess 28(1):17–27

Tessier Y, Lovejoy S, Schertzer D (1993) Universal multifractals: theory and observations for rain and clouds. J Appl Meteorol 32:223–250